Rapid Communications

Stabilization of the skyrmion crystal phase and transport in thin-film antiferromagnets

Ricardo Zarzuela,[1] Se Kwon Kim,[1,2] and Yaroslav Tserkovnyak[1]
[1]*Department of Physics and Astronomy, University of California, Los Angeles, California 90095, USA*
[2]*Department of Physics and Astronomy, University of Missouri, Columbia, Missouri 65211, USA*

(Received 26 June 2018; revised manuscript received 26 August 2019; published 18 September 2019)

We investigate the stability and dynamics of the skyrmion lattice in antiferromagnetic thin films subjected to fieldlike torques such as, e.g., those induced by an electric current in CuMnAs and Mn_2Au via the inverse spin-galvanic effect. The skyrmion crystal phase represents the ground state of the antiferromagnet in a substantial area of the phase diagram, the latter being parametrized by the effective staggered field and uniaxial anisotropy constant. Experimental signatures of the skyrmion crystal phase and readout schemes based on topological transport (e.g., the spin Hall effect) are discussed. We also estimate qualitatively the effect of thermal and current fluctuations, including shot noise, on the stability of the skyrmion lattice.

DOI: 10.1103/PhysRevB.100.100408

Introduction. Two-dimensional skyrmions [1] arise in spin systems with broken inversion symmetry and spin-orbit coupling [2,3] and have been observed in a plethora of ferromagnets over the last decade [4–7]. These topological excitations are protected against structural distortions and moderate external perturbations [8], exhibit a particlelike behavior [9,10], carry quanta of topological charge, and have received much attention recently due to their potential usage as building blocks for logic devices and information/energy storage [11–16], controllable nucleation/annihilation by local spin-polarized current injection [17], low current threshold for depinning [18], and unconventional transport properties such as the skyrmion Hall effect [19,20]. Along with the Abrikosov vortex lattice in type-II superconductors [21], the skyrmion crystal (SkX) stands out as almost the only well-understood example of a soliton lattice, therefore illustrating the crystal order beyond the usual atomic/molecular paradigm.

Antiferromagnets, which display ultrafast (within the THz range) spin dynamics and produce minimal stray fields, offer promising perspectives to exploit and control skyrmions. This scenario has been explored recently, yielding intrinsically different dynamics [22–25] from those found for ferromagnetic skyrmions but qualitatively similar results on the topological robustness and the nucleation/annihilation (by spin currents) [26,27]. A distinctive dynamical feature of antiferromagnetic (AFM) skyrmions is the absence of a gyrotropic response, which leads in particular to significantly larger terminal velocities [23,24] as compared to the ferromagnetic case, an attractive feature from the technological standpoint. Nevertheless, the direct observation of any AFM skyrmion phase remains elusive, since the staggered order parameter couples weakly to electromagnetic fields and, therefore, AFM textures are generally challenging to drive or read out.

Hitherto, it is largely unknown whether the SkX phase can be stabilized in thin-film antiferromagnets [28] and, if so, which of its macroscopic signatures are accessible experimentally. Further insight into these questions is thus vital to boost progress in the field of skyrmionics. In this Rapid Communication, we explore different possibilities to utilize fieldlike torques for the stabilization of the SkX phase in quasi-two-dimensional AFM films. Fieldlike torques emulate a Zeeman coupling for the Néel order $\boldsymbol{l}$ at the level of energetics $\mathcal{E}_Z[\boldsymbol{l}] = -\boldsymbol{l}\cdot\mathcal{B}_{sg}$, where $\mathcal{B}_{sg}$ denotes the staggered field. Generically, there are two possible ways of inducing this staggered field: first, by endowing an effective ferromagnetism in the system whose magnetization is collinear with the Néel order, such that $\mathcal{B}_{sg}$ is proportional to an applied magnetic field. One example of this is engendered by the magnetoelectric effect in Cr_2O_3 [29,30]. Second, by preserving the AFM nature of the system and breaking (structural) symmetries that allow the onset of the staggered field via electrically induced spin torques. This is the relevant scenario for Mn_2Au and CuMnAs subjected to an electrical current, where the staggered field is induced by the inverse spin-galvanic effect and reads $\mathcal{B}_{sg} = \xi\,\hat{c}\times\vec{j}$. Here, $\vec{j}$ denotes the current density, $\hat{c}$ is the tetragonal c axis along which inversion symmetry is locally broken, and ξ is the charge current-to-magnetic field ratio [31,32].

Our starting point is thus based on the effective free-energy density

$$\mathcal{E}_{\rm eff}[\boldsymbol{l}] = \frac{A}{2}(\vec{\nabla}\boldsymbol{l})^2 + D(l_z\vec{\nabla}\cdot\boldsymbol{l} - \boldsymbol{l}\cdot\vec{\nabla}l_z) - \mathcal{B}_{sg}l_z + \frac{\mathcal{K}}{2}l_z^2 + \frac{K_c}{2}|\hat{z}\cdot(\vec{\nabla}\times\boldsymbol{l})|^2, \quad (1)$$

describing AFM films with broken reflection symmetry along the normal to the basal (xy) plane and retaining axial symmetry around the z axis (see Fig. 1). The terms on the right-hand side represent, from left to right, the exchange interaction, the interfacial Dzyaloshinskii-Moriya (DM) interaction [33–35], the Zeeman-like term (with the staggered field lying along the normal to the film), the effective uniaxial anisotropy (along the z axis), and the so-called *compass* term [3], an anisotropic exchangelike interaction arising microscopically from Rashba physics (the same as the DM term). Note that the compass and DM terms respect the symmetry apropos of simultaneous spin and spatial rotations about the z axis, but break it with respect to pure spin rotations. We show that the skyrmion lattice is

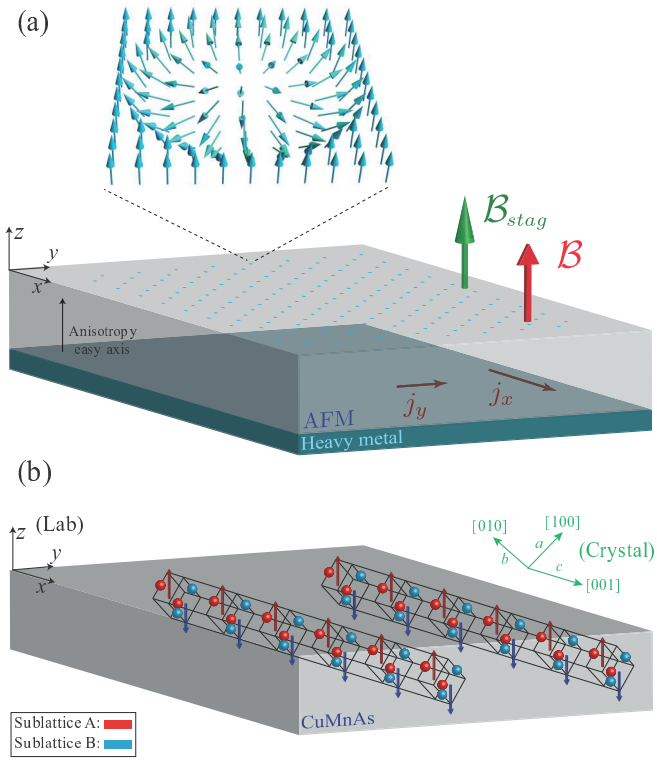

FIG. 1. AFM thin film deposited on a heavy-metal substrate. (a) The MCA axis lies along the normal to the film. Blue dots depict skyrmions located at the sites of the static hexagonal lattice. Inset: Spatial dependence of the staggered order parameter for an isolated Néel skyrmion. (b) Crystallographic structure of the CuMnAs sample. The film is grown along the [110] direction. Red/blue spheres illustrate Mn atoms belonging to different magnetic sublattices, whereas red/blue arrows denote the direction of the resultant staggered field.

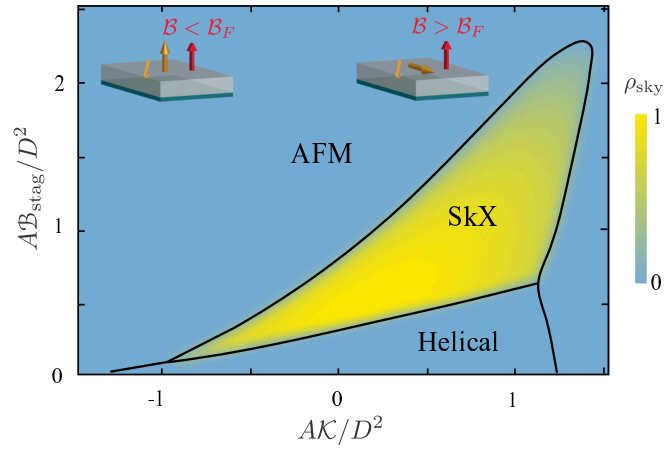

FIG. 2. Zero-temperature phase diagram in the anisotropy-staggered field phase space $(\mathcal{K}, \mathcal{B}_{\rm sg})$, obtained from a circular-cell minimization of the energy (1). The AFM film has an effective easy-axis (easy-plane) anisotropy for $\mathcal{K} < 0$ ($\mathcal{K} > 0$). The insets show the spatial configuration of the Néel order (yellow arrow) within the AFM phase. The averaged skyrmion density $\rho_{\rm sky}$ is measured in arbitrary units.

the ground state in a substantial area of the parameter space, possessing thus a large degree of tunability. Furthermore, we discuss the effect of thermal and current fluctuations on the stability of the phase diagram and propose the readout of the skyrmion crystal via the spin Hall response of conduction electrons in metallic antiferromagnets and nonlocal magnetotransport measurements [36] in AFM insulators.

Effective theory. Within the exchange approximation, Eq. (1) encapsulates the minimal model describing quasi-two-dimensional antiferromagnets for the geometry depicted in Fig. 1, namely, the magnetocrystalline-anisotropy (MCA) axis and staggered/external magnetic fields normal to the film. We consider hereafter films sufficiently thin so that the uniformity of the Néel order along the z axis can be safely assumed. The exchange is described by the stiffness constant A and the effective anisotropy contains the intrinsic MCA (on-site uniaxial constant K) and a term rooted in the weak coupling of the Néel order to the external magnetic field $\mathcal{B}$; it is parametrized by the constant $\mathcal{K}(\mathcal{B}) = K + \chi\mathcal{B}^2$, where χ denotes the (transverse) spin susceptibility of the film. Note that for $K < 0$ (easy-axis antiferromagnet) our minimal model undergoes the spin-flop transition at $\mathcal{B}_F = \sqrt{|K|/\chi}$, where $\mathcal{K}$ flips its sign. Fieldlike torques $\boldsymbol{\tau}_{\rm FL} = \boldsymbol{l} \times \mathcal{B}_{\rm sg}$ arise when sublattice symmetry is broken and, within the Landau-Lifshitz-Gilbert framework for AFM dynamics, their effect can be captured by the nonequilibrium Zeeman-like energy functional $\mathcal{E}_{\rm Z}$ [37]. The Lifshitz invariant $l_z\vec{\nabla}\cdot\boldsymbol{l} - \boldsymbol{l}\cdot\vec{\nabla}l_z$ describes the interfacial DM interaction induced by the heavy-metal substrate, which breaks reflection symmetry along the z axis, and D denotes the Dzyaloshinskii coupling constant. Furthermore, for materials in which global centrosymmetry is broken, additional bulk DM terms $D_{\rm b}\,\boldsymbol{l}\cdot(\vec{\nabla}\times\boldsymbol{l})$ would arise, which we will not include in our analysis.

This model, as we will elucidate below, stabilizes Néel skyrmions [see the inset of Fig. 1(a)], which are classified by the following integer invariant (the so-called topological charge) providing a measure of the wrapping of the AFM order around the unit sphere,

$$\mathcal{Q}_{\rm sky} = \int d^2\vec{r}\,\rho_{\rm sky}, \qquad \rho_{\rm sky} = -\frac{1}{4\pi}\boldsymbol{l}\cdot(\partial_x\boldsymbol{l}\times\partial_y\boldsymbol{l}). \tag{2}$$

It is worth remarking that, in the absence of the DM energy term, skyrmions are unstable according to the Hobart-Derrick's scaling argument [42]. Collapse of these solitons into atomic-size defects is prevented by the DM interaction, which introduces a characteristic length scale below which spatial fluctuations of the texture (in particular, shrinking) are energetically penalized. In particular, zero-field minimization of Eq. (1) for the rigid hard cutoff ansatz for skyrmions with $|\mathcal{Q}_{\rm sky}| = 1$ yields the radius $R_\star \simeq 2\pi D/K$ [43].

Stability and phase diagram. Interplay between exchange, anisotropy, and DM interactions enables the stabilization of individual AFM skyrmions. This is not the case for the SkX phase, which also requires the polarizing effect of the staggered field on the Néel order. Figure 2 illustrates the phase diagram of the AFM thin film at zero temperature in the parameter space $(\mathcal{K}, \mathcal{B}_{\rm sg})$, which contains the (uniform) AFM, helical, and SkX phases. It has been computed along the lines of Ref. [3], assuming in particular a hexagonal lattice structure for the SkX phase with a circularly symmetric

variational ansatz for Néel skyrmions. We note in passing that microscopic reasoning based on the Rashba model gives rise to $K_c \sim D^2/2A$ and that, for the rigid skyrmion ansatz, our compass term drops out. The skyrmion lattice is found to be the ground state in a substantial area of the phase diagram: The two first-order phase transitions helical $\Rightarrow$ SkX $\Rightarrow$ AFM are fomented when the staggered field is swept since Eq. (1) describes the energetics of a ferromagnetic film with the broken reflection symmetry normal to the basal plane [44]. Remarkably, in the spin-flop region ($\mathcal{B} > \mathcal{B}_F$) the SkX phase is more robust and occupies a wider area than that of $0 \leqslant \mathcal{B} < \mathcal{B}_F$ (effective easy-axis antiferromagnet). We observe that our phase diagram looks qualitatively the same as that of Ref. [3], from which we conclude that compass terms do not contribute relevantly to the stabilization of the phases involved in Fig. 2.

One consequence of Eq. (2) is that sublattice and time-reversal symmetries must break down to generate a net skyrmion charge in the AFM film [26]. This symmetry breaking occurs in the presence of $\mathcal{B}_{\rm sg}$, which acts as a Zeeman field setting a preferred polarization (along the z axis) for the order parameter [45]. Note that isolated skyrmions represent magnetic excitations emerging in a uniform AFM ground state (gas phase). This metastability is characterized by an energy barrier of topological origin, which in turn translates into a finite lifetime for AFM skyrmions [23,46]. On the contrary, the skyrmion lattice is a thermodynamic phase *per se*.

Experimental platforms. Tetragonal CuMnAs and Mn_2Au, in which inversion symmetry is locally broken and the two magnetic sublattices $\{A, B\}$ form inversion partners, epitomize the class of AFM metals exhibiting the Edelstein spin-orbit torque (ESOT) [31,32]. A charge current $\vec{j}$ injected in the *ab* plane generates, via the inverse spin-galvanic (Edelstein) effect, an in-plane (local) spin polarization transverse to it whose sign flips between the two AFM sublattices [see Fig. 1(b)]. An exchange interaction between this nonequilibrium polarization and the sublattice spins yields an effective staggered field $\mathcal{B}_{\rm sg} = \xi\, \hat{c} \times \vec{j}$ that couples linearly to the Néel order. Regarding the MCA of these materials, with bulk *ab*-plane biaxial anisotropy, we invoke the reduced symmetries resulting from the quasi-two-dimensionality of the films: Ref. [47] reports the uniaxial character (easy axis along one of the $\langle 110 \rangle$ crystal axis) of the MCA in CuMnAs samples with thicknesses <10 nm. Furthermore, the heavy-metal substrate also contributes to the MCA of the heterostructure with a uniaxial term (easy axis normal to the interface). Note that the latter is the most generic anisotropy always arising at interfaces and certainly will dominate in some cases (e.g., thin films and strong spin-orbit interactions).

For the sake of concreteness, we consider CuMnAs thin films with a (110) basal plane deposited on a heavy-metal substrate. The magnetic field and charge current are applied normal to and within the (110) plane, respectively [see Fig. 1(a)]. The component of $\vec{j}$ transverse to the c axis (referred to as the x direction hereafter), which will be fixed in our setup, is responsible for the ESOT stabilizing the SkX phase, whereas the other independent (and tunable) component j_x will be utilized to drive the dynamics of the skyrmion lattice. We note in passing that we can control the axes of the phase diagram by changing j_y (staggered field) and the external magnetic field (uniaxial anisotropy); this real-time controllability allows us to explore the entire phase diagram with one sample. *Ab initio* calculations of the ESOT in CuMnAs yield values for the staggered field of the order of 10 mT per current densities $\sim 10^7$ A/cm^2 [32], leading to the value $\xi = 10^{-9}$ T cm^2/A for the charge current-to-magnetic field ratio. Critical staggered fields for the nucleation (helical $\Rightarrow$ SkX) and annihilation (SkX $\Rightarrow$ AFM) of the skyrmion lattice lie in the range [0.12,0.65] and [0.12,2.30], respectively (in units of D^2/A), when the external magnetic field is swept (see Fig. 2). With account of the estimates $J_{\rm CuMnAs} \sim 40$ meV for the exchange constant [48] and $D \sim 2$ mJ/m^2 for the bulk DM strength induced by a Pt substrate [49], the SkX phase becomes stable in a 5-nm CuMnAs thin film for $\mathcal{B}_{\rm sg}$ in the range of 30–155 mT or, equivalently, for charge currents in the range of 10^7–10^8 A/cm^2. Note that these currents are accessible experimentally (see, e.g., Ref. [50], where current densities up to 10^9 A/cm^2 are applied to CuMnAs) without compromising the integrity of the heterostructure by Joule heating.

Other possible platforms are chromia (α-Cr_2O_3) thin films and antiferromagnet–hard ferromagnet bilayers subjected to spin exchange. The former exhibits a (magnetoelectrically induced) surface magnetization below the Néel temperature [29], which, strikingly, is collinear with the Néel order. Therefore, an external magnetic field engenders a Zeeman torque for the AFM dynamics of chromia through the boundaries [51]. In the latter, the Néel order can be controlled via the exchange bias effect [52–54], with the magnetization of the ferromagnet (taken to be fully spin polarized) playing the role of the staggered field. This effect is also interfacial and will be enhanced for uncompensated surfaces and thin AFM films.

Transport. Current-driven steady motion of skyrmions in the gas phase is described by the center-of-mass velocity $\partial_t \vec{\Re}|_{\rm t} = -\zeta_\parallel^{\rm gas}\, \vec{j} - \zeta_\perp^{\rm gas}\, \hat{e}_z \times \vec{j}$, where $\zeta_\parallel^{\rm gas} = \vartheta_1/\alpha s$, $\zeta_\perp^{\rm gas} = \vartheta_2 \mathcal{Q}_{\rm sky}/\alpha s \mathcal{I}$, $\mathcal{I} = \int d^2\vec{r}(\partial_x \vec{l} \cdot \partial_x \vec{l})/4\pi$ is a dimensionless geometric factor, α denotes the Gilbert damping constant, s is the saturated spin density and ϑ_1, ϑ_2 are phenomenological constants parametrizing the dissipative and reactive components of the spin-transfer torque, respectively [51]. Similarly, the current-induced terminal velocity of the skyrmion lattice reads $\partial_t u_x|_{\rm t} = -\zeta_\parallel^{\rm gas} j_x + \zeta_\perp^{\rm gas} j_y$ and $\partial_t u_y|_{\rm t} = -p(\zeta_\perp^{\rm gas} j_x + \zeta_\parallel^{\rm gas} j_y)$ for a slab geometry along the x direction, where $\vec{u}\,[\vec{r}, t] = (u_x, u_y)$ are the collective coordinates describing, in the continuum limit, the displacement of the lattice sites with respect to their equilibrium positions, and $p < 1$ is a dimensionless prefactor quantifying the loss of angular momentum via spin pumping [37].

Itinerant electrons in AFM metals experience, in the adiabatic limit for spin dynamics, a fictitious electromagnetic field $\mathcal{B}_z = \pm h\rho_{\rm sky}/e$, $\vec{E} = \mathcal{B}_z\, \hat{e}_z \times \partial_t \vec{u}$ when flowing within the skyrmion crystal [55,56], where e is the electron charge and the sign $\pm$ corresponds to the spin-up (spin-down) bands with respect to $\boldsymbol{l}$. Note that we have disregarded other terms originating in Rasbha (spin-orbit) physics and spin-flip processes [57]. In the internal spin frame of reference (adjusted to the local Néel order), the SkX phase engenders the spin Hall current

$$\vec{\mathcal{J}}_z = \pi(\hbar/e)^2 \mu\, \rho_{\rm sky}\, \hat{e}_z \times (ne\, \partial_t \vec{u}|_{\rm t} - \vec{j}), \tag{3}$$

where n, μ, and $m_\star$ denote the concentration, mobility, and effective mass of conduction electrons, respectively [37,58]. This spin Hall response can be understood as two copies of the topological Hall effect [59] corresponding to the spin-up (spin-down) bands. The spin Hall current generated by the skyrmion texture can be detected, via the inverse spin Hall effect, by attaching a heavy metal to the sides of the AFM film; it reads $\langle(\boldsymbol{l}\cdot\hat{\boldsymbol{e}}_z)\vec{\mathcal{J}}_z\rangle_{\rm int}$ and is polarized along the (laboratory) z axis, with $\langle\cdots\rangle_{\rm int}$ denoting the spatial average over the lateral interface. Note that these adjacent contacts are different from the heavy-metal substrate shown in Fig. 1 that is used for inducing an interfacial DM interaction. It is worth remarking here that an additional anomalous contribution to the spin Hall current arises from the nontrivial Berry curvature of the Bloch bands [60].

Fluctuations and disorder. Our mean-field treatment for the phase diagram, based on the Landau expansion of the free-energy functional given by Eq. (1), can break down as a result of fluctuations. For instance, spin fluctuations can give rise to the melting of the SkX phase via elastic breakdown of the soliton lattice due to unbinding of dislocations. From the general theories for the two-dimensional lattice melting developed in Refs. [61–65], the melting temperature of the SkX phase reads $T_m=\zeta A$, where the dimensionless prefactor ζ accounts for the strength of the weak substrate disorder and the renormalization of the Lamé coefficients of the skyrmion crystal. In this expression, we used the estimates $\lambda_0,\mu_0\sim D^2/A$, [40] and $a\sim A/D$ for the bare Lamé coefficients and the lattice spacing, respectively, from which we obtain $\lambda_0 a^2=\mu_0 a^2\sim A$; T_m scales linearly with the exchange stiffness constant, and therefore may be as high as a fraction of the Néel temperature. Furthermore, for weak disorder we would expect a glassy behavior such as that of the Abrikosov flux lattice in type-II superconductors [66] or even a Bragg glass phase [67,68] due to the quasi-two-dimensionality of the AFM films considered.

Current fluctuations contribute, via the inverse spin-galvanic effect, to the dissipation of energy in the SkX phase: The Johnson-Nyquist noise for the (driving) electric field, characterized by the correlator $\langle\delta E(\vec{r},t)\delta E(\vec{r}\,',t')\rangle=4k_BT\rho\,\delta(\vec{r}-\vec{r}\,')\delta(t-t')$ [69], leads to an enhancement of the net Gilbert-type damping of the Néel dynamics, in the form of an anisotropic tensor $\hat{\alpha}_{\rm JN}\sim 2\gamma^2\xi^2 s/\rho$, where ρ and γ are the resistivity and the gyromagnetic ratio, respectively [71,72]. With account of the value $\rho=160\,\mu\Omega\,$cm for a disordered sample of CuMnAs [73], we obtain the estimate $|\hat{\alpha}_{\rm JN}|\simeq 0.01\sim\alpha_0$, where α_0 denotes the bare Gilbert damping constant. Since $\alpha_{\rm tot}\sim 2\alpha_0\ll 1$, current fluctuations are insignificant from the point of view of the phase diagram as they do not affect spectral properties of the antiferromagnet. Because of that, we can still use bare parameters in Eq. (1) and, therefore, the theory for the AFM SkX phase should be well described by this effective free energy.

Discussion. The minimal free-energy model discussed here does not capture the physics of the spin Hall and spin-transfer torques allowed by the symmetries of our device geometry [74]. It remains as an open question to elucidate how these torques affect the phase diagram, which requires the exploration of the ensuing Néel dynamics in the framework of the theory of dynamical phase transitions. A second open problem concerns the effect of shot noise on the stability of the thermodynamic phases depicted in Fig. 2. Let us make the following rough estimate based on the relevance of shot noise for electrical current fluctuations, which comes down to comparing the voltage drop $U_{\rm in}$ over the inelastic length scale $l_{\rm in}$ to the system temperature [75,76]: Thermal noise will dominate when $eU_{\rm in}<k_BT$ and, in the presence of an electric current, this voltage drop can be roughly estimated as $U_{\rm in}\sim\rho j l_{\rm in}$. By taking the values $j=10^7$ A/cm^2 and $l_{\rm in}\approx 100$ nm [77], we obtain the crossover temperature $T_{\rm in}\approx 200$ K. Therefore, shot noise may be disregarded as long as the temperature is higher than $T_{\rm in}$; at lower temperatures, however, shot noise will start dominating and its stochastic aspects need to be taken into consideration. In this regard, it remains as an open issue to elucidate whether shot noise significantly affects the dynamical phase diagram of our heterostructure near the crossover temperature.

Spin currents offer a knob to inject and drive AFM skyrmions within the insulating medium, similar to the ferromagnetic case [36,43]. In that regard, a two-terminal geometry enables the pumping of topological charge into the antiferromagnet via the spin-transfer effect. Nonlocal magnetotransport (spin drag) measurements could therefore be used to (i) probe the existence of these topological textures, and (ii) discriminate the gas and SkX phases, since the drag coefficient exhibits a different dependence on the staggered field [36]. In the metallic scenario, measurement of the spin Hall current generated by the (mobile) skyrmion lattice via the inverse spin Hall effect in the adjacent heavy-metal terminals would provide further experimental evidence of AFM skyrmions in a crystal phase. Other experimental techniques well suited to read out the skyrmion crystal could be the x-ray magnetic linear dichroism (XMLD) imaging, the spin-transfer-torque ferromagnetic resonance, and the noncollinear magnetoresistance [78].

Acknowledgments. We thank J. Sinova for insightful discussions on the Mn_2Au and CuMnAs platforms. This work has been supported by NSF under Grant No. DMR-1742928. R.Z. thanks Fundación Ramón Areces for support through a postdoctoral fellowship within the XXVII Convocatoria de Becas para Ampliación de Estudios en el Extranjero en Ciencias de la Vida y de la Materia.

[1] A. A. Belavin and A. M. Polyakov, JETP Lett. **22**, 245 (1975).
[2] A. N. Bogdanov, U. K. Rossler, M. Wolf, and K.-H. Muller, Phys. Rev. B **66**, 214410 (2002).
[3] S. Banerjee, J. Rowland, O. Erten, and M. Randeria, Phys. Rev. X **4**, 031045 (2014).
[4] S. Mühlbauer, B. Binz, F. Jonietz, C. Pfleiderer, A. Rosch, A. Neubauer, R. Georgii, and P. Böni, Science **323**, 915 (2009).
[5] X. Z. Yu, Y. Onose, N. Kanazawa, J. H. Park, J. H. Han, Y. Matsui, N. Nagaosa, and Y. Tokura, Nature (London) **465**, 901 (2010).

[6] S. Seki, X. Z. Yu, S. Ishiwata, and Y. Tokura, Science **336**, 198 (2012).

[7] W. Jiang, P. Upadhyaya, W. Zhang, G. Yu, M. B. Jungfleisch, F. Y. Fradin, J. E. Pearson, Y. Tserkovnyak, K. L. Wang, O. Heinonen, S. G. E. te Velthuis, and A. Hoffmann, Science **349**, 283 (2015).

[8] S. Rohart, J. Miltat, and A. Thiaville, Phys. Rev. B **93**, 214412 (2016).

[9] S. Pöllath, J. Wild, L. Heinen, T. N. G. Meier, M. Kronseder, L. Tutsch, A. Bauer, H. Berger, C. Pfleiderer, J. Zweck, A. Rosch, and C. H. Back, Phys. Rev. Lett. **118**, 207205 (2017).

[10] S.-Z. Lin, C. Reichhardt, C. D. Batista, and A. Saxena, Phys. Rev. B **87**, 214419 (2013).

[11] A. Fert, V. Cros, and J. Sampaio, Nat. Nanotechnol. **8**, 152 (2013).

[12] Y. Zhou and M. Ezawa, Nat. Commun. **5**, 4652 (2014).

[13] X. Zhang, M. Ezawa, and Y. Zhou, Sci. Rep. **5**, 9400 (2015).

[14] M.-C. Chen and K. Roy, arXiv:1705.01095.

[15] A. Fert, N. Reyren, and V. Cros, Nat. Rev. Mater. **2**, 17031 (2017).

[16] Y. Tserkovnyak and J. Xiao, Phys. Rev. Lett. **121**, 127701 (2018).

[17] J. Sampaio, V. Cros, S. Rohart, A. Thiaville, and A. Fert, Nat. Nanotechnol. **8**, 839 (2013).

[18] N. Nagaosa and Y. Tokura, Nat. Nanotechnol. **8**, 899 (2013), and references therein.

[19] W. Jiang, X. Zhang, G. Yu, W. Zhang, X. Wang, M. B. Jungfleisch, J. E. Pearson, X. Cheng, O. Heinonen, K. L. Wang, Y. Zhou, A. Hoffmann, and S. G. E. te Velthuis, Nat. Phys. **13**, 162 (2017).

[20] K. Litzius, I. Lemesh, B. Krüger, P. Bassirian, L. Caretta, K. Richter, F. Büttner, K. Sato, O. A. Tretiakov, J. Förster, R. M. Reeve, M. Weigand, I. Bykova, H. Stoll, G. Schütz, G. S. D. Beach, and Mathias Kläui, Nat. Phys. **13**, 170 (2017).

[21] A. A. Abrikosov, Zh. Eksp. Teor. Fiz. **32**, 1442 (1957) [JETP **5**, 1174 (1957)].

[22] S. K. Kim, O. Tchernyshyov, and Y. Tserkovnyak, Phys. Rev. B **92**, 020402(R) (2015).

[23] J. Barker and O. A. Tretiakov, Phys. Rev. Lett. **116**, 147203 (2016).

[24] H. Velkov, O. Gomonay, M. Beens, G. Schwiete, A. Brataas, J. Sinova, and R. A. Duine, New J. Phys. **18**, 075016 (2016).

[25] C. Jin, C. Song, J. Wang, and Q. Liu, Appl. Phys. Lett. **109**, 182404 (2016).

[26] R. Keesman, M. Raaijmakers, A. E. Baerends, G. T. Barkema, and R. A. Duine, Phys. Rev. B **94**, 054402 (2016).

[27] X. Zhang, Y. Zhou, and M. Ezawa, Sci. Rep. **6**, 24795 (2016).

[28] A. Bogdanov and A. Shestakov, Phys. Solid State **40**, 1350 (1998).

[29] X. He, Y. Wang, N. Wu, A. N. Caruso, E. Vescovo, K. D. Belashchenko, P. A. Dowben, and Ch. Binek, Nat. Mater. **9**, 579 (2010).

[30] K. D. Belashchenko, O. Tchernyshyov, A. A. Kovalev, and O. A. Tretiakov, Appl. Phys. Lett. **108**, 132403 (2016).

[31] J. Železný, H. Gao, K. Výborný, J. Zemen, J. Mašek, A. Manchon, J. Wunderlich, J. Sinova, and T. Jungwirth, Phys. Rev. Lett. **113**, 157201 (2014).

[32] P. Wadley, B. Howells, J. Železný, C. Andrews, V. Hills, R. P. Campion, V. Novák, K. Olejník, F. Maccherozzi, S. S. Dhesi, S. Y. Martin, T. Wagner, J. Wunderlich, F. Freimuth, Y. Mokrousov, J. Kuneš, J. S. Chauhan, M. J. Grzybowski, A. W. Rushforth, K. W. Edmonds, B. L. Gallagher, and T. Jungwirth, Science **351**, 587 (2016).

[33] I. E. Dzyaloshinskii, Zh. Eksp. Teor. Fiz. **32**, 1547 (1957) [JETP **5**, 1259 (1957)].

[34] T. Moriya, Phys. Rev. **120**, 91 (1960).

[35] I. E. Dzyaloshinskii, Zh. Eksp. Teor. Fiz. **46**, 1420 (1964) [JETP **19**, 960 (1964)].

[36] H. Ochoa, S.-K. Kim, O. Tchernyshyov, and Y. Tserkovnyak, Phys. Rev. B **96**, 020410(R) (2017).

[37] See Supplemental Material at http://link.aps.org/supplemental/10.1103/PhysRevB.100.100408 for further details into the effect of fieldlike torques on the AFM dynamics, for a derivation of the equation of motion for skyrmions within the collective variable approach in the SkX phase, and for a semiclassical calculation of the induced spin current, which includes Refs. [36,38–41].

[38] A. Auerbach, *Interacting Electrons and Quantum Magnetism* (Springer, New York, 1994); S. Sachdev, *Quantum Phase Transitions* (Cambridge University Press, Cambridge, UK, 1999).

[39] S.-Z. Lin, Phys. Rev. B **96**, 014407 (2017).

[40] O. Petrova and O. Tchernyshyov, Phys. Rev. B **84**, 214433 (2011).

[41] E. M. Chudnovsky, Phys. Rev. Lett. **99**, 206601 (2007).

[42] R. H. Hobart, Proc. Phys. Soc. **82**, 201 (1963); G. M. Derrick, J. Math. Phys. **5**, 1252 (1964).

[43] H. Ochoa, S. K. Kim, and Y. Tserkovnyak, Phys. Rev. B **94**, 024431 (2016).

[44] A. Bogdanov and A. Hubert, J. Magn. Magn. Mater. **138**, 255 (1994).

[45] Sublattice symmetry can also break down at the interface with the heavy metal and/or at the structural level (defects, etc.).

[46] P. Bessarab, D. Yudin, D. R. Gulevich, P. Wadley, M. Titov, and O. A. Tretiakov, Phys. Rev. B **99**, 140411 (2019).

[47] P. Wadley, V. Hills, M. R. Shahedkhah, K. W. Edmonds, R. P. Campion, V. Novák, B. Ouladdiaf, D. Khalyavin, S. Langridge, V. Saidl, P. Nemec, A. W. Rushforth, B. L. Gallagher, S. S. Dhesi, F. Maccherozzi, J. Železný, and T. Jungwirth, Sci. Rep. **5**, 17079 (2015).

[48] V. Baltz, A. Manchon, M. Tsoi, T. Moriyama, T. Ono, and Y. Tserkovnyak, Rev. Mod. Phys. **90**, 015005 (2018).

[49] C.-F. Pai, M. Mann, A. J. Tan, and G. S. D. Beach, Phys. Rev. B **93**, 144409 (2016).

[50] K. Olejník, T. Seifert, Z. Kašpar, V. Novák, P. Wadley, R. P. Campion, M. Baumgartner, P. Gambardella, P. Němec, J. Wunderlich, J. Sinova, P. Kužel, M. Müller, T. Kampfrath, and T. Jungwirth, Sci. Adv. **4**, eaar3566 (2018).

[51] R. Zarzuela, S. K. Kim, and Y. Tserkovnyak, Phys. Rev. B **97**, 014418 (2018).

[52] B. G. Park, J. Wunderlich, X. Martí, V. Holý, Y. Kurosaki, M. Yamada, H. Yamamoto, A. Nishide, J. Hayakawa, H. Takahashi, A. B. Shick, and T. Jungwirth, Nat. Mater. **10**, 347 (2011).

[53] J. Wu, D. Carlton, J. S. Park, Y. Meng, E. Arenholz, A. Doran, A. T. Young, A. Scholl, C. Hwang, H. W. Zhao, J. Bokor, and Z. Q. Qiu, Nat. Phys. **7**, 303 (2011).

[54] G. Yu, A. Jenkins, X. Ma, S. A. Razavi, C. He, G. Yin, Q. Shao, Q. He, H. Wu, W. Li, W. Jiang, X. Han, X. Li, A. C. Bleszynski Jayich, P. K. Amiri, and K. L. Wang, Nano Lett. **18**, 980 (2018).

[55] R. Cheng and Q. Niu, Phys. Rev. B **86**, 245118 (2012).

[56] We have considered for simplicity the case in which elec-

trons keep their spins parallel or antiparallel to the Néel-order background without any deviation. This is equivalent to assuming that the intersublattice band mixing yields corrections at the subleading order to the orientation of the electron spins with respect to the Néel order, and therefore are disregarded. In other words, $|t_{AB}| \ll J'$, where t_{AB} and J' denote the intersublattice hopping term and the electron-texture exchange constant, respectively. This situation may arise, for example, in layered AFM systems such as Mn_2Au and CuMnAs (see Ref. [57]).

[57] Y. Yamane, J. Ieda, and J. Sinova, Phys. Rev. B **93**, 180408(R) (2016).

[58] C. A. Akosa, O. A. Tretiakov, G. Tatara, and A. Manchon, Phys. Rev. Lett. **121**, 097204 (2018).

[59] P. Bruno, V. K. Dugaev, and M. Taillefumier, Phys. Rev. Lett. **93**, 096806 (2004).

[60] B. Göbel, A. Mook, J. Henk, and I. Mertig, Phys. Rev. B **96**, 060406(R) (2017).

[61] V. L. Berezinskii, Zh. Eksp. Teor. Fiz. **59**, 907 (1971) [JETP **32**, 493 (1971)].

[62] J. M. Kosterlitz and D. J. Thouless, J. Phys. C **6**, 1181 (1973).

[63] D. R. Nelson and B. I. Halperin, Phys. Rev. B **19**, 2457 (1979).

[64] A. P. Young, Phys. Rev. B **19**, 1855 (1979).

[65] D. Carpentier and P. Le Doussal, Phys. Rev. Lett. **81**, 1881 (1998).

[66] G. Blatter, M. V. Feigel'man, V. B. Geshkenbein, A. I. Larkin, and V. M. Vinokur, Rev. Mod. Phys. **66**, 1125 (1994).

[67] T. Giamarchi and P. Le Doussal, Phys. Rev. B **52**, 1242 (1995).

[68] P. Le Doussal and T. Giamarchi, Physica C **331**, 233 (2000).

[69] Note that we have neglected Coulomb correlation effects in this expression for the sake of simplicity. In the generic (interacting) scenario, the spatial correlator acquires a nonlocal character (see Ref. [70]).

[70] C. H. Wong and Y. Tserkovnyak, Phys. Rev. B **81**, 060404(R) (2010).

[71] J. Foros, A. Brataas, Y. Tserkovnyak, and G. E. W. Bauer, Phys. Rev. B **78**, 140402(R) (2008).

[72] Y. Tserkovnyak and C. H. Wong, Phys. Rev. B **79**, 014402 (2009).

[73] F. Máca, J. Kudrnovský, V. Drchal, K. Carva, P. Baláž, and I. Turek, Phys. Rev. B **96**, 094406 (2017).

[74] R. Zarzuela and Y. Tserkovnyak, Phys. Rev. B **95**, 180402(R) (2017).

[75] Ya. M. Blanter and M. Büttiker, Phys. Rep. **336**, 1 (2000).

[76] For the sake of simplicity, we describe shot noise by means of a single scattering length scale l_{in}.

[77] V. P. Zhukov, E. V. Chulkov, and P. M. Echenique, Phys. Rev. B **73**, 125105 (2006).

[78] C. Hanneken, F. Otte, A. Kubetzka, B. Dupé, N. Romming, K. von Bergmann, R. Wiesendanger, and S. Heinze, Nat. Nanotechnol. **10**, 1039 (2015).